Title	First measurements of absolute branching fractions of the Ξ_c^0 baryon at Belle
Author(s)	Li Y. B., Tanida Kiyoshi, Belle Collaboration, 161 of others
Citation	Physical Review Letters,122(8),p.082001_1-082001_7
Text Version	Published Journal Article
URL	https://jopss.jaea.go.jp/search/servlet/search?5067923
DOI	https://doi.org/10.1103/PhysRevLett.122.082001
Right	Published by the American Physical Society under the terms of the Creative Commons Attribution 4.0 International license. Further distribution of this work must maintain attribution to the author(s) and the published article's title, journal citation, and DOI. Funded by SCOAP^3.

PHYSICAL REVIEW LETTERS **122,** 082001 (2019)

First Measurements of Absolute Branching Fractions of the Ξ_c^0 Baryon at Belle

Y. B. Li,[69] C. P. Shen,[2,10] C. Z. Yuan,[26] I. Adachi,[17,13] H. Aihara,[84] S. Al Said,[79,35] D. M. Asner,[3] T. Aushev,[54] R. Ayad,[79] I. Badhrees,[79,34] Y. Ban,[69] V. Bansal,[67] C. Beleño,[12] M. Berger,[76] V. Bhardwaj,[21] B. Bhuyan,[22] T. Bilka,[5] J. Biswal,[31] A. Bondar,[4,65] A. Bozek,[62] M. Bračko,[48,31] L. Cao,[32] D. Červenkov,[5] A. Chen,[59] B. G. Cheon,[15] K. Chilikin,[43] K. Cho,[37] S.-K. Choi,[14] Y. Choi,[77] D. Cinabro,[88] S. Cunliffe,[8] S. Di Carlo,[41] Z. Doležal,[5] T. V. Dong,[17,13] Z. Drásal,[5] S. Eidelman,[4,65,43] J. E. Fast,[67] B. G. Fulsom,[67] R. Garg,[68] V. Gaur,[87] N. Gabyshev,[4,65] A. Garmash,[4,65] A. Giri,[23] P. Goldenzweig,[32] D. Greenwald,[81] B. Grube,[81] K. Hayasaka,[64] H. Hayashii,[58] C.-L. Hsu,[78] T. Iijima,[56,55] K. Inami,[55] G. Inguglia,[8] A. Ishikawa,[82] R. Itoh,[17,13] M. Iwasaki,[66] Y. Iwasaki,[17] W. W. Jacobs,[25] S. Jia,[2] Y. Jin,[84] D. Joffe,[33] K. K. Joo,[6] G. Karyan,[8] T. Kawasaki,[36] H. Kichimi,[17] D. Y. Kim,[75] H. J. Kim,[40] J. B. Kim,[38] K. T. Kim,[38] S. H. Kim,[15] K. Kinoshita,[7] P. Kodyš,[5] S. Korpar,[48,31] D. Kotchetkov,[16] P. Križan,[44,31] R. Kroeger,[51] P. Krokovny,[4,65] T. Kumita,[86] A. Kuzmin,[4,65] Y.-J. Kwon,[90] J. Y. Lee,[73] S. C. Lee,[40] L. K. Li,[26] L. Li Gioi,[49] J. Libby,[24] D. Liventsev,[87,17] M. Lubej,[31] J. MacNaughton,[52] M. Masuda,[83] T. Matsuda,[52] M. Merola,[28,57] K. Miyabayashi,[58] H. Miyata,[64] R. Mizuk,[43,53,54] G. B. Mohanty,[80] R. Mussa,[29] E. Nakano,[66] M. Nakao,[17,13] K. J. Nath,[22] M. Nayak,[88,17] M. Niiyama,[39] S. Nishida,[17,13] H. Ono,[63,64] Y. Onuki,[84] P. Pakhlov,[43,53] G. Pakhlova,[43,54] B. Pal,[3] S. Pardi,[28] S.-H. Park,[90] S. Paul,[81] T. K. Pedlar,[46] R. Pestotnik,[31] L. E. Piilonen,[87] V. Popov,[43,54] E. Prencipe,[19] G. Russo,[28] Y. Sakai,[17,13] M. Salehi,[47,45] S. Sandilya,[7] L. Santelj,[17] T. Sanuki,[82] V. Savinov,[70] O. Schneider,[42] G. Schnell,[1,20] J. Schueler,[16] C. Schwanda,[27] A. J. Schwartz,[7] Y. Seino,[64] K. Senyo,[89] M. E. Sevior,[50] T.-A. Shibata,[85] J.-G. Shiu,[61] B. Shwartz,[4,65] E. Solovieva,[43,54] M. Starič,[31] M. Sumihama,[11] T. Sumiyoshi,[86] W. Sutcliffe,[32] M. Takizawa,[74,18,71] K. Tanida,[30] Y. Tao,[9] F. Tenchini,[8] K. Trabelsi,[17,13] M. Uchida,[85] T. Uglov,[43,54] Y. Unno,[15] S. Uno,[17,13] P. Urquijo,[50] R. Van Tonder,[32] G. Varner,[16] B. Wang,[7] C. H. Wang,[60] M.-Z. Wang,[61] P. Wang,[26] X. L. Wang,[10] E. Won,[38] S. B. Yang,[38] H. Ye,[8] J. Yelton,[9] J. H. Yin,[26] Y. Yusa,[64] Z. P. Zhang,[72] V. Zhilich,[4,65] and V. Zhukova[43]

(Belle Collaboration)

[1]*University of the Basque Country UPV/EHU, 48080 Bilbao*
[2]*Beihang University, Beijing 100191*
[3]*Brookhaven National Laboratory, Upton, New York 11973*
[4]*Budker Institute of Nuclear Physics SB RAS, Novosibirsk 630090*
[5]*Faculty of Mathematics and Physics, Charles University, 121 16 Prague*
[6]*Chonnam National University, Kwangju 660-701*
[7]*University of Cincinnati, Cincinnati, Ohio 45221*
[8]*Deutsches Elektronen–Synchrotron, 22607 Hamburg*
[9]*University of Florida, Gainesville, Florida 32611*
[10]*Key Laboratory of Nuclear Physics and Ion-beam Application (MOE) and Institute of Modern Physics, Fudan University, Shanghai 200443*
[11]*Gifu University, Gifu 501-1193*
[12]*II. Physikalisches Institut, Georg-August-Universität Göttingen, 37073 Göttingen*
[13]*SOKENDAI (The Graduate University for Advanced Studies), Hayama 240-0193*
[14]*Gyeongsang National University, Chinju 660-701*
[15]*Hanyang University, Seoul 133-791*
[16]*University of Hawaii, Honolulu, Hawaii 96822*
[17]*High Energy Accelerator Research Organization (KEK), Tsukuba 305-0801*
[18]*J-PARC Branch, KEK Theory Center, High Energy Accelerator Research Organization (KEK), Tsukuba 305-0801*
[19]*Forschungszentrum Jülich, 52425 Jülich*
[20]*IKERBASQUE, Basque Foundation for Science, 48013 Bilbao*
[21]*Indian Institute of Science Education and Research Mohali, SAS Nagar, 140306*
[22]*Indian Institute of Technology Guwahati, Assam 781039*
[23]*Indian Institute of Technology Hyderabad, Telangana 502285*
[24]*Indian Institute of Technology Madras, Chennai 600036*
[25]*Indiana University, Bloomington, Indiana 47408*
[26]*Institute of High Energy Physics, Chinese Academy of Sciences, Beijing 100049*
[27]*Institute of High Energy Physics, Vienna 1050*

[28]*INFN—Sezione di Napoli, 80126 Napoli*
[29]*INFN—Sezione di Torino, 10125 Torino*
[30]*Advanced Science Research Center, Japan Atomic Energy Agency, Naka 319-1195*
[31]*J. Stefan Institute, 1000 Ljubljana*
[32]*Institut für Experimentelle Teilchenphysik, Karlsruher Institut für Technologie, 76131 Karlsruhe*
[33]*Kennesaw State University, Kennesaw, Georgia 30144*
[34]*King Abdulaziz City for Science and Technology, Riyadh 11442*
[35]*Department of Physics, Faculty of Science, King Abdulaziz University, Jeddah 21589*
[36]*Kitasato University, Sagamihara 252-0373*
[37]*Korea Institute of Science and Technology Information, Daejeon 305-806*
[38]*Korea University, Seoul 136-713*
[39]*Kyoto University, Kyoto 606-8502*
[40]*Kyungpook National University, Daegu 702-701*
[41]*LAL, Univ. Paris-Sud, CNRS/IN2P3, Université Paris-Saclay, Orsay 91405*
[42]*École Polytechnique Fédérale de Lausanne (EPFL), Lausanne 1015*
[43]*P.N. Lebedev Physical Institute of the Russian Academy of Sciences, Moscow 119991*
[44]*Faculty of Mathematics and Physics, University of Ljubljana, 1000 Ljubljana*
[45]*Ludwig Maximilians University, 80539 Munich*
[46]*Luther College, Decorah, Iowa 52101*
[47]*University of Malaya, 50603 Kuala Lumpur*
[48]*University of Maribor, 2000 Maribor*
[49]*Max-Planck-Institut für Physik, 80805 München*
[50]*School of Physics, University of Melbourne, Victoria 3010*
[51]*University of Mississippi, University, Mississippi 38677*
[52]*University of Miyazaki, Miyazaki 889-2192*
[53]*Moscow Physical Engineering Institute, Moscow 115409*
[54]*Moscow Institute of Physics and Technology, Moscow Region 141700*
[55]*Graduate School of Science, Nagoya University, Nagoya 464-8602*
[56]*Kobayashi-Maskawa Institute, Nagoya University, Nagoya 464-8602*
[57]*Università di Napoli Federico II, 80055 Napoli*
[58]*Nara Women's University, Nara 630-8506*
[59]*National Central University, Chung-li 32054*
[60]*National United University, Miao Li 36003*
[61]*Department of Physics, National Taiwan University, Taipei 10617*
[62]*H. Niewodniczanski Institute of Nuclear Physics, Krakow 31-342*
[63]*Nippon Dental University, Niigata 951-8580*
[64]*Niigata University, Niigata 950-2181*
[65]*Novosibirsk State University, Novosibirsk 630090*
[66]*Osaka City University, Osaka 558-8585*
[67]*Pacific Northwest National Laboratory, Richland, Washington 99352*
[68]*Panjab University, Chandigarh 160014*
[69]*Peking University, Beijing 100871*
[70]*University of Pittsburgh, Pittsburgh, Pennsylvania 15260*
[71]*Theoretical Research Division, Nishina Center, RIKEN, Saitama 351-0198*
[72]*University of Science and Technology of China, Hefei 230026*
[73]*Seoul National University, Seoul 151-742*
[74]*Showa Pharmaceutical University, Tokyo 194-8543*
[75]*Soongsil University, Seoul 156-743*
[76]*Stefan Meyer Institute for Subatomic Physics, Vienna 1090*
[77]*Sungkyunkwan University, Suwon 440-746*
[78] *School of Physics, University of Sydney, New South Wales 2006*
[79]*Department of Physics, Faculty of Science, University of Tabuk, Tabuk 71451*
[80]*Tata Institute of Fundamental Research, Mumbai 400005*
[81]*Department of Physics, Technische Universität München, 85748 Garching*
[82]*Department of Physics, Tohoku University, Sendai 980-8578*
[83]*Earthquake Research Institute, University of Tokyo, Tokyo 113-0032*
[84]*Department of Physics, University of Tokyo, Tokyo 113-0033*
[85]*Tokyo Institute of Technology, Tokyo 152-8550*
[86]*Tokyo Metropolitan University, Tokyo 192-0397*
[87]*Virginia Polytechnic Institute and State University, Blacksburg, Virginia 24061*
[88]*Wayne State University, Detroit, Michigan 48202*

[89]*Yamagata University, Yamagata 990-8560*
[90]*Yonsei University, Seoul 120-749*

(Received 24 November 2018; revised manuscript received 27 January 2019; published 25 February 2019)

We present the first measurements of absolute branching fractions of Ξ_c^0 decays into $\Xi^-\pi^+$, $\Lambda K^-\pi^+$, and $pK^-K^-\pi^+$ final states. The measurements are made using a dataset comprising $(772 \pm 11) \times 10^6$ $B\bar{B}$ pairs collected at the $\Upsilon(4S)$ resonance with the Belle detector at the KEKB e^+e^- collider. We first measure the absolute branching fraction for $B^- \to \bar{\Lambda}_c^-\Xi_c^0$ using a missing-mass technique; the result is $\mathcal{B}(B^- \to \bar{\Lambda}_c^-\Xi_c^0) = (9.51 \pm 2.10 \pm 0.88) \times 10^{-4}$. We subsequently measure the product branching fractions $\mathcal{B}(B^- \to \bar{\Lambda}_c^-\Xi_c^0)\mathcal{B}(\Xi_c^0 \to \Xi^-\pi^+)$, $\mathcal{B}(B^- \to \bar{\Lambda}_c^-\Xi_c^0)\mathcal{B}(\Xi_c^0 \to \Lambda K^-\pi^+)$, and $\mathcal{B}(B^- \to \bar{\Lambda}_c^-\Xi_c^0)\mathcal{B}(\Xi_c^0 \to pK^-K^-\pi^+)$ with improved precision. Dividing these product branching fractions by the result for $B^- \to \bar{\Lambda}_c^-\Xi_c^0$ yields the following branching fractions: $\mathcal{B}(\Xi_c^0 \to \Xi^-\pi^+) = (1.80 \pm 0.50 \pm 0.14)\%$, $\mathcal{B}(\Xi_c^0 \to \Lambda K^-\pi^+) = (1.17 \pm 0.37 \pm 0.09)\%$, and $\mathcal{B}(\Xi_c^0 \to pK^-K^-\pi^+) = (0.58 \pm 0.23 \pm 0.05)\%$. For the above branching fractions, the first uncertainties are statistical and the second are systematic. Our result for $\mathcal{B}(\Xi_c^0 \to \Xi^-\pi^+)$ can be combined with Ξ_c^0 branching fractions measured relative to $\Xi_c^0 \to \Xi^-\pi^+$ to yield other absolute Ξ_c^0 branching fractions.

DOI: 10.1103/PhysRevLett.122.082001

Half a century after the theory of quantum chromodynamics (QCD) was developed, understanding the nonperturbative property of the strong interaction still remains a challenge. Weak decays of charmed hadrons play a unique role in the study of strong interactions, as the charm mass scale is near the boundary between perturbative and nonperturbative QCD. The charmed-baryon sector offers an excellent laboratory for testing heavy-quark symmetry and light-quark chiral symmetry, both of which have important implications for the low-energy dynamics of heavy baryons interacting with Goldstone bosons [1]. In exclusive charm decays, the heavy-quark expansion does not work, and experimental data are needed to extract nonperturbative quantities in the decay amplitudes [2–5]. Decays of charmed baryons with an additional quark and spin of 1/2 provide complementary information to that of charm-meson decays.

Unlike in the charmed-meson sector, where D^0, D^+, and D_s^+ decays are all well measured, in the charm-baryon sector only Λ_c^+ absolute branching fractions have been measured [6,7]. Thus, the branching fractions of Ξ_c^0 baryons are all measured relative to the $\Xi_c^0 \to \Xi^-\pi^+$ mode. Thus a measurement of the absolute branching fraction $\mathcal{B}(\Xi_c^0 \to \Xi^-\pi^+)$ is needed to determine the absolute branching fractions of other Ξ_c^0 decays. In charmed-baryon decays, nonfactorizable contributions to the decay amplitude are important, and a variety of models have been developed to predict the decay rate in such processes [8–17]. For example, the $\mathcal{B}(\Xi_c^0 \to \Xi^-\pi^+)$ has been predicted to be 0.74% or 1.12% [15], $(2.24 \pm 0.34)\%$ [16], and $(1.91 \pm 0.17)\%$ [17]. Experimental information is crucial to validate these models as well as to constrain the model parameters.

The $\mathcal{B}(\Xi_c^0 \to \Lambda K^-\pi^+)$ and $\mathcal{B}(\Xi_c^0 \to pK^-K^-\pi^+)$ have been measured relative to $\mathcal{B}(\Xi_c^0 \to \Xi^-\pi^+)$ to be $1.07 \pm 0.12 \pm 0.07$ and $0.33 \pm 0.03 \pm 0.03$ [18], respectively. The decay $\Xi_c^0 \to pK^-K^-\pi^+$ plays a key role in many bottom-baryon studies at LHCb [19,20]. The decay $B^- \to \bar{\Lambda}_c^-\Xi_c^0$, which proceeds via a $b \to c\bar{c}s$ transition, has a branching fraction predicted to be of the order 10^{-3} [21]. However, this has not been measured because the absolute branching fractions of Ξ_c^0 are unknown. The measured product branching fractions are $\mathcal{B}(B^- \to \bar{\Lambda}_c^-\Xi_c^0)\mathcal{B}(\Xi_c^0 \to \Xi^-\pi^+) = (2.4 \pm 0.9) \times 10^{-5}$ and $\mathcal{B}(B^- \to \bar{\Lambda}_c^-\Xi_c^0)\mathcal{B}(\Xi_c^0 \to \Lambda K^-\pi^+) = (2.1 \pm 0.9) \times 10^{-5}$ [22–24].

In this Letter, we perform an analysis of $B^- \to \bar{\Lambda}_c^-\Xi_c^0$ with $\bar{\Lambda}_c^-$ reconstructed via $\bar{p}K^+\pi^-$ and $\bar{p}K_S^0$ modes, and Ξ_c^0 reconstructed both inclusively and exclusively via $\Xi^-\pi^+$, $\Lambda K^-\pi^+$, and $pK^-K^-\pi^+$ modes [25]. We present first a measurement of the absolute branching fraction for $B^- \to \bar{\Lambda}_c^-\Xi_c^0$ using a missing-mass technique. For this analysis we fully reconstruct the tag-side B^+ decay. We subsequently measure the product branching fractions $\mathcal{B}(B^- \to \bar{\Lambda}_c^-\Xi_c^0)\mathcal{B}(\Xi_c^0 \to \Xi^-\pi^+)$, $\mathcal{B}(B^- \to \bar{\Lambda}_c^-\Xi_c^0)\mathcal{B}(\Xi_c^0 \to \Lambda K^-\pi^+)$, and $\mathcal{B}(B^- \to \bar{\Lambda}_c^-\Xi_c^0)\mathcal{B}(\Xi_c^0 \to pK^-K^-\pi^+)$. For these measurements we do not reconstruct the recoiling B^+ decay, as the signal decays are fully reconstructed. Dividing these product branching fractions by $\mathcal{B}(B^- \to \bar{\Lambda}_c^-\Xi_c^0)$ yields the branching fractions $\mathcal{B}(\Xi_c^0 \to \Xi^-\pi^+)$, $\mathcal{B}(\Xi_c^0 \to \Lambda K^-\pi^+)$, and $\mathcal{B}(\Xi_c^0 \to pK^-K^-\pi^+)$.

This analysis is based on the full data sample of 702.6 fb^{-1} collected at the $\Upsilon(4S)$ resonance by the Belle detector [26] at the KEKB asymmetric-energy

---

e^+e^- collider [27]. The detector is described in detail elsewhere [26].

To optimize signal selection criteria and calculate the signal reconstruction efficiency, we use Monte Carlo (MC) simulated events. Signal events of B meson decays are generated using EVTGEN [28], while inclusive Ξ_c^0 decays are generated using PYTHIA [29]. The MC events are processed with a detector simulation based on GEANT3 [30]. MC samples of $\Upsilon(4S) \to B\bar{B}$ events with $B = B^+$ or B^0, and $e^+e^- \to q\bar{q}$ events with $q = u, d, s, c$ at $\sqrt{s} = 10.58$ GeV, are used as background samples.

To select signal candidates, well-reconstructed tracks and particle identification are performed using the same method as in Ref. [31], as well as the $\Lambda \to p\pi^-$ and $K_S^0 \to \pi^+\pi^-$ candidates [31].

For the inclusive analysis of the Ξ_c^0 decay, the tag-side B^+ meson candidate, $B^+_{\rm tag}$, is reconstructed using a neural network based on a full hadron-reconstruction algorithm [32]. Each $B^+_{\rm tag}$ candidate has an associated output value $O_{\rm NN}$ from the multivariate analysis that ranges from 0 to 1. A candidate with larger $O_{\rm NN}$ is more likely to be a true B meson. If multiple $B^+_{\rm tag}$ candidates are found in an event, the candidate with the largest $O_{\rm NN}$ is selected. To improve the purity of the $B^+_{\rm tag}$ sample, we require $O_{\rm NN} > 0.005$, $M_{\rm bc}^{\rm tag} > 5.27$ GeV$/c^2$, and $|\Delta E^{\rm tag}| < 0.04$ GeV, where the latter two intervals correspond to approximately 3σ in resolution. The variables $M_{\rm bc}^{\rm tag}$ and $\Delta E^{\rm tag}$ are defined as $M_{\rm bc}^{\rm tag} \equiv \sqrt{E_{\rm beam}^2 - |\sum_i \vec{p}_i^{\,\rm tag}|^2}$ and $\Delta E^{\rm tag} \equiv \sum_i E_i^{\rm tag} - E_{\rm beam}$, where $E_{\rm beam} \equiv \sqrt{s}/2$ is the beam energy and $(E_i^{\rm tag}, \vec{p}_i^{\,\rm tag})$ is the four-momentum of the $B^+_{\rm tag}$ daughter i in the e^+e^- center-of-mass system (c.m.s.). After reconstructing a $B^+_{\rm tag}$ candidate, $\bar{\Lambda}_c^- \to \bar{p}K^+\pi^-$ and $\bar{\Lambda}_c^- \to \bar{p}K_S^0$ decays are reconstructed from among the remaining tracks. We perform a fit for the decay vertex and require that $\chi^2_{\rm vertex}/{\rm n.d.f.} < 15$, where n.d.f. is the number of degrees of freedom. If there is more than one $\bar{\Lambda}_c^-$ candidate in an event, the candidate with the smallest $\chi^2_{\rm vertex}/{\rm n.d.f.}$ is selected. We define a $\bar{\Lambda}_c^-$ signal region $|M_{\bar{p}K^+\pi^-/\bar{p}K_S^0} - m_{\bar{\Lambda}_c^-}| < 10$ MeV$/c^2$ (3.0σ), where $m_{\bar{\Lambda}_c^-}$ is the nominal mass of the $\bar{\Lambda}_c^-$ [22].

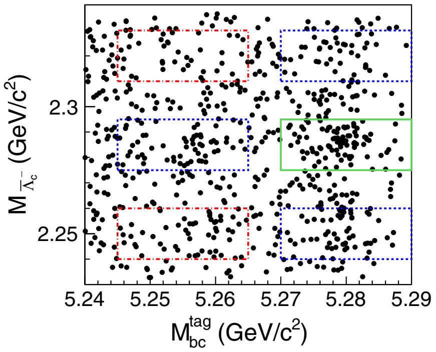

FIG. 1. The distribution of $M_{\rm bc}^{\rm tag}$ of $B^+_{\rm tag}$ versus $M_{\bar{\Lambda}_c^-}$ of selected $B^- \to \bar{\Lambda}_c^- \Xi_c^0$ candidates with $\Xi_c^0 \to$ anything, summed over the two reconstructed $\bar{\Lambda}_c^-$ decay modes. The solid box shows the signal region, and the dashed and dash-dotted boxes define the $M_{\rm bc}^{\rm tag}$ and $M_{\bar{\Lambda}_c^-}$ sidebands described in the text.

The "recoil mass" of the daughter X in $B^- \to \bar{\Lambda}_c^- + X$ is calculated using $M^{\rm recoil}_{B^+_{\rm tag}\bar{\Lambda}_c^-} = \sqrt{(P_{\rm c.m.s} - P_{B^+_{\rm tag}} - P_{\bar{\Lambda}_c^-})^2}$, where $P_{\rm c.m.s}$, $P_{B^+_{\rm tag}}$, and $P_{\bar{\Lambda}_c^-}$ are the four-momenta of the initial e^+e^- system, the tagged B^+ meson, and the reconstructed $\bar{\Lambda}_c^-$ baryon. To improve the recoil mass resolution, we use $M^{\rm rec}_{B^+_{\rm tag}\bar{\Lambda}_c^-} \equiv M^{\rm recoil}_{B^+_{\rm tag}\bar{\Lambda}_c^-} + M_{B^+_{\rm tag}} - m_B + M_{\bar{\Lambda}_c^-} - m_{\bar{\Lambda}_c^-}$, where $M_{B^+_{\rm tag}}$ is the invariant mass of the $B^+_{\rm tag}$ candidate, $M_{\bar{\Lambda}_c^-}$ is the reconstructed mass of the $\bar{\Lambda}_c^-$ candidate, and m_B is the nominal mass of the B meson [22]. The distribution of $M_{\rm bc}^{\rm tag}$ of the $B^+_{\rm tag}$ candidates versus $M_{\bar{\Lambda}_c^-}$ of the selected $B^- \to \bar{\Lambda}_c^- \Xi_c^0$ signal candidates summed over the two reconstructed $\bar{\Lambda}_c^-$ decay modes is shown in Fig. 1, for $2.40 < M^{\rm rec}_{B^+_{\rm tag}\bar{\Lambda}_c^-} < 2.53$ GeV$/c^2$. We observe a significant excess of $B^- \to \bar{\Lambda}_c^- \Xi_c^0$ candidates in the signal region denoted as the solid box in Fig. 1. To check for possible peaking backgrounds, we define $M_{\rm bc}^{\rm tag}$ and $M_{\bar{\Lambda}_c^-}$ sidebands, represented by the dashed and dash-dotted boxes in Fig. 1. Each sideband box is the same size as the signal box. The background contribution in the signal box is estimated using half the number of events in the blue dashed sideband boxes minus one-fourth the number of events in the red dash-dotted sideband boxes. The $M^{\rm rec}_{B^+_{\rm tag}\bar{\Lambda}_c^-}$ distribution of events in both the signal and sideband boxes is shown in Fig. 2. No peaking backgrounds in the studied recoil Ξ_c^0 mass region are found in the $M_{\rm bc}^{\rm tag}$ and $M_{\bar{\Lambda}_c^-}$ sideband events, as shown with the shaded histogram in Fig. 2.

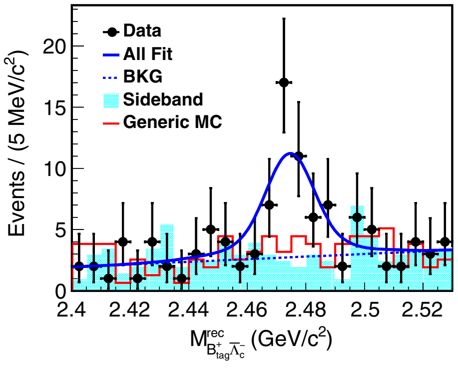

FIG. 2. The fit to the $M^{\rm rec}_{B^+_{\rm tag}\bar{\Lambda}_c^-}$ distribution of the selected candidate events. The points with error bars represent the data, the solid blue curve is the best fit, the dashed curve is the fitted background (BKG), the cyan shaded histogram is from the scaled $M_{\rm bc}^{\rm tag}$ and $M_{\bar{\Lambda}_c^-}$ sidebands, the red open histogram is from the sum of the MC-simulated contributions from the $e^+e^- \to q\bar{q}$ with $q = u, d, s, c$, and $\Upsilon(4S) \to B\bar{B}$ generic-decay backgrounds with the number of events normalized to the number of events from the normalized $M_{\rm bc}^{\rm tag}$ and $M_{\bar{\Lambda}_c^-}$ sidebands.

To extract the Ξ_c^0 signal yield, an unbinned maximum-likelihood fit is performed to the $M^{\rm rec}_{B^+_{\rm tag}\bar{\Lambda}_c^-}$ distribution. A double-Gaussian function (its parameters are fixed to those from a fit to the MC-simulated signal distribution) is used to model the Ξ_c^0 signal shape, and a first-order polynomial is taken as the background shape. The fit results are shown in Fig. 2.

The fitted Ξ_c^0 signal yield is $N_{\Xi_c^0} = 40.9 \pm 9.0$, with a statistical significance of 5.5σ. The significance is calculated using $\sqrt{-2\ln(\mathcal{L}_0/\mathcal{L}_{\rm max})}$, where $\mathcal{L}_0$ and $\mathcal{L}_{\rm max}$ are the likelihoods of the fits without and with a signal component, respectively. The $\mathcal{B}(B^- \to \bar{\Lambda}_c^- \Xi_c^0)$ is calculated using $N_{\Xi_c^0}/[N_{B^-}(\varepsilon_1\mathcal{B}_1 + \varepsilon_2\mathcal{B}_2)]$. In this expression, $\mathcal{B}_1 = \mathcal{B}(\bar{\Lambda}_c^- \to \bar{p}K^+\pi^-)$, $\mathcal{B}_2 = \mathcal{B}(\bar{\Lambda}_c^- \to \bar{p}K_S^0)\mathcal{B}(K_S^0 \to \pi^+\pi^-)$, and $N_{B^-} = 2N_{\Upsilon(4S)}\mathcal{B}[\Upsilon(4S) \to B^+B^-]$, where $N_{\Upsilon(4S)}$ is the number of $\Upsilon(4S)$ events, and the $\mathcal{B}[\Upsilon(4S) \to B^+B^-] = (51.4 \pm 0.6)\%$ [22]. The reconstruction efficiencies ε_1 and ε_2 of the two $\bar{\Lambda}_c^-$ decay modes are obtained from MC simulation. The $\mathcal{B}(\bar{\Lambda}_c^- \to \bar{p}K^+\pi^-)$, $\mathcal{B}(\bar{\Lambda}_c^- \to \bar{p}K_S^0)$, and $\mathcal{B}(K_S^0 \to \pi^+\pi^-)$ are taken from Ref. [22]. The result is $\mathcal{B}(B^- \to \bar{\Lambda}_c^- \Xi_c^0) = [9.51 \pm 2.10({\rm stat})] \times 10^{-4}$.

For the analysis of the exclusive Ξ_c^0 decays, we again use $B^- \to \bar{\Lambda}_c^- \Xi_c^0$ decays in which $\bar{\Lambda}_c^- \to (\bar{p}K^+\pi^-, \bar{p}K_S^0)$. However, instead of reconstructing the tag-side $B^+_{\rm tag}$, we fully reconstruct the Ξ_c^0 decay in the final states $\Xi^-\pi^+$, $\Lambda K^-\pi^+$, and $pK^-K^-\pi^+$, where $\Xi^- \to \Lambda\pi^-$ and $\Lambda \to p\pi^-$. Fits to the B^-, Ξ_c^0, and Ξ^- decay vertices are performed. If there is more than one B^- candidate in an event, the one with the smallest $\chi^2_{\rm vertex}$/n.d.f. from the B^- vertex fit is selected. We subsequently require $\chi^2_{\rm vertex}$/n.d.f. < 50, 15, and 15 for reconstructed B^-, Ξ_c^0, and Ξ^- candidates, respectively. The Ξ^- and Ξ_c^0 signal ranges are defined as $|M_{\Lambda\pi^-} - m_{\Xi^-}| < 10$ MeV$/c^2$ and $|M_{\Xi_c^0} - m_{\Xi_c^0}| < 20$ MeV$/c^2$ (3.0σ), where $M_{\Lambda\pi^-}$ and $M_{\Xi_c^0}$ are the invariant masses of the selected Ξ^- and Ξ_c^0 candidates, and m_{Ξ^-} and $m_{\Xi_c^0}$ are the nominal masses of Ξ^- and Ξ_c^0 [22]. The $\bar{\Lambda}_c^-$ signal interval is the same as in the inclusive analysis of Ξ_c^0 decays. The B^- signal candidates are identified using the beam-energy-constrained mass $M_{\rm bc}$ and the energy difference ΔE, where $M_{\rm bc}$ and ΔE are calculated in the same manner as done for $B^+_{\rm tag}$ candidates, but, here, tracks from the B^- signal candidate decay are used.

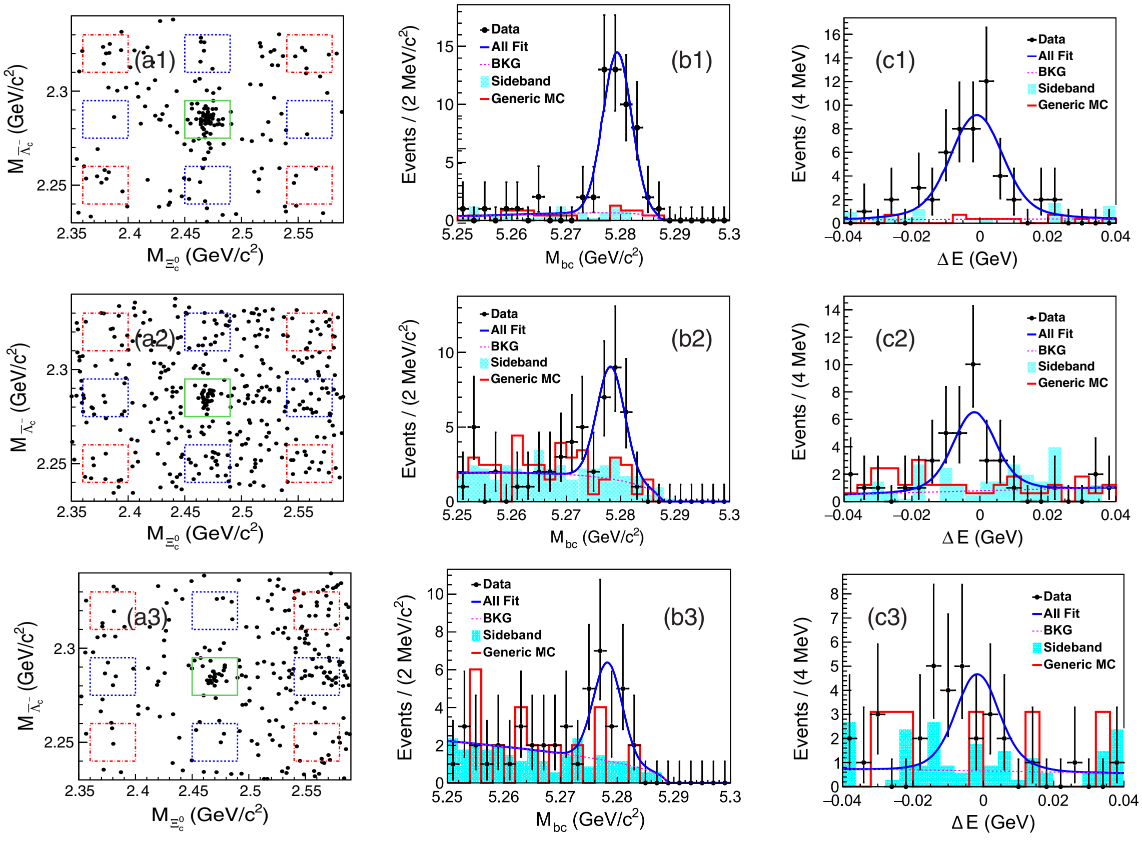

FIG. 3. The distributions of $M_{\Xi_c^0}$ versus $M_{\bar{\Lambda}_c^-}$ (a) and the fits to the $M_{\rm bc}$ (b) and ΔE (c) distributions of the selected $B^- \to \bar{\Lambda}_c^- \Xi_c^0$ candidates with $\Xi_c^0 \to \Xi^-\pi^+$ (1), $\Xi_c^0 \to \Lambda K^-\pi^+$ (2), and $\Xi_c^0 \to pK^-K^-\pi^+$ (3) decays, summed over the two reconstructed $\bar{\Lambda}_c^-$ decay modes. In (a), the central solid box defines the signal region. The red dash-dotted and blue dashed boxes show the $M_{\Xi_c^0}$ and $M_{\bar{\Lambda}_c^-}$ sideband regions used for the estimation of the non-Ξ_c^0 and non-$\bar{\Lambda}_c^-$ backgrounds (see text). In (b) and (c), the dots with error bars represent the data, the blue solid curves represent the best fits, and the dashed curves represent the fitted background contributions. The shaded and red open histograms have the same meaning as in Fig. 2.

TABLE I. Summary of the measured branching fractions and ratios of Ξ_c^0 decays (last column), and the corresponding systematic uncertainties (%). For the branching fractions and ratios, the first uncertainties are statistical and the second are systematic.

Observable	Efficiency	Fit	Λ_c decays	B_{tag}	$N_{B^{\pm}}$	Sum	Measured value
$\mathcal{B}(B^- \to \bar{\Lambda}_c^- \Xi_c^0)$	3.46	4.80	5.51	4.2	1.82	9.3	$(9.51 \pm 2.10 \pm 0.88) \times 10^{-4}$
$\mathcal{B}(B^- \to \bar{\Lambda}_c^- \Xi_c^0)\mathcal{B}(\Xi_c^0 \to \Xi^- \pi^+)$	4.74	3.49	5.75	⋯	1.82	8.4	$(1.71 \pm 0.28 \pm 0.15) \times 10^{-5}$
$\mathcal{B}(B^- \to \bar{\Lambda}_c^- \Xi_c^0)\mathcal{B}(\Xi_c^0 \to \Lambda K^- \pi^+)$	4.56	4.03	5.82	⋯	1.82	8.6	$(1.11 \pm 0.26 \pm 0.10) \times 10^{-5}$
$\mathcal{B}(B^- \to \bar{\Lambda}_c^- \Xi_c^0)\mathcal{B}(\Xi_c^0 \to p K^- K^- \pi^+)$	7.25	5.11	5.03	⋯	1.82	10.5	$(5.47 \pm 1.78 \pm 0.57) \times 10^{-6}$
$\mathcal{B}(\Xi_c^0 \to \Xi^- \pi^+)$	2.94	5.9	⋯	4.2	⋯	7.8	$(1.80 \pm 0.50 \pm 0.14)\%$
$\mathcal{B}(\Xi_c^0 \to \Lambda K^- \pi^+)$	2.65	6.3	⋯	4.2	⋯	8.0	$(1.17 \pm 0.37 \pm 0.09)\%$
$\mathcal{B}(\Xi_c^0 \to p K^- K^- \pi^+)$	3.84	7.0	⋯	4.2	⋯	9.0	$(0.58 \pm 0.23 \pm 0.05)\%$
$\mathcal{B}(\Xi_c^0 \to \Lambda K^- \pi^+)/\mathcal{B}(\Xi_c^0 \to \Xi^- \pi^+)$	1.36	5.3	⋯	⋯	⋯	5.5	$0.65 \pm 0.18 \pm 0.04$
$\mathcal{B}(\Xi_c^0 \to p K^- K^- \pi^+)/\mathcal{B}(\Xi_c^0 \to \Xi^- \pi^+)$	5.24	6.2	⋯	⋯	⋯	8.1	$0.32 \pm 0.12 \pm 0.07$

We define a B^- signal region as $M_{\text{bc}} > 5.27\ \text{GeV}/c^2$ and $|\Delta E| < 0.03$ GeV. The distributions of $M_{\Xi_c^0}$ versus $M_{\bar{\Lambda}_c^-}$ for events in the B^- signal region are shown in Figs. 3(a1)–3(a3) after all selection criteria are applied. The central solid boxes define the Ξ_c^0 and $\bar{\Lambda}_c^-$ signal regions. The backgrounds from non-Ξ_c^0 and non-$\bar{\Lambda}_c^-$ events are estimated from $M_{\Xi_c^0}$ and $M_{\bar{\Lambda}_c^-}$ sidebands, represented by the dashed boxes in Figs. 3(a1)–3(a3). The sideband's contribution is estimated similarly to the inclusive analysis. Figures 3(b) and 3(c) show the M_{bc} and ΔE distributions in the Ξ_c^0 and $\bar{\Lambda}_c^-$ signal regions from the selected $B^- \to \bar{\Lambda}_c^- \Xi_c^0$ candidates with (1) $\Xi_c^0 \to \Xi^- \pi^+$, (2) $\Xi_c^0 \to \Lambda K^- \pi^+$, and (3) $\Xi_c^0 \to p K^- K^- \pi^+$. All distributions are summed over the two reconstructed $\bar{\Lambda}_c^-$ decay modes.

The number of $B^- \to \bar{\Lambda}_c^- \Xi_c^0$ signal events is extracted by performing an unbinned two-dimensional maximum-likelihood fit to the M_{bc} versus ΔE distributions. For the M_{bc} distribution, the signal shape is modeled with a Gaussian function and the background is described using an ARGUS function [33]. For the ΔE distribution, the signal shape is modeled using a double-Gaussian function and the background is described by a first-order polynomial. All shape parameters of the signal functions are fixed to the values obtained from the fits to the MC-simulated signal distributions. The fit results are shown in Fig. 3.

We obtain $N_{\Xi^- \pi^+} = 44.8 \pm 7.3$, $N_{\Lambda K^- \pi^+} = 24.1 \pm 5.5$, and $N_{p K^- K^- \pi^+} = 16.6 \pm 5.4$ signal events with statistical significances of 9.5σ, 6.8σ, and 4.6σ. Using the efficiencies calculated from MC simulation, we obtain $\mathcal{B}(B^- \to \bar{\Lambda}_c^- \Xi_c^0)\mathcal{B}(\Xi_c^0 \to \Xi^- \pi^+) = [1.71 \pm 0.28(\text{stat})] \times 10^{-5}$, $\mathcal{B}(B^- \to \bar{\Lambda}_c^- \Xi_c^0)\mathcal{B}(\Xi_c^0 \to \Lambda K^- \pi^+) = [1.11 \pm 0.26(\text{stat})] \times 10^{-5}$, and $\mathcal{B}(B^- \to \bar{\Lambda}_c^- \Xi_c^0)\mathcal{B}(\Xi_c^0 \to p K^- K^- \pi^+) = [5.47 \pm 1.78(\text{stat})] \times 10^{-6}$.

There are several sources of systematic uncertainties as listed in Table I. The reconstruction-efficiency-related uncertainties include those for tracking efficiency (0.35% per track), particle identification efficiency (0.9% per kaon, 0.9% per pion, and 3.6% per proton), as well as Λ (3.0% [34]) and K_S^0 (1.6% [35]) reconstruction efficiencies. Assuming that all the above sources of systematic uncertainty are independent, the reconstruction-efficiency-related uncertainties are summed in quadrature for each decay mode, yielding 4.0%–8.4%, depending on the specific decay mode. For the four branching-fraction measurements, the final uncertainties related to the efficiency of the reconstruction are summed in quadrature over the two reconstructed $\bar{\Lambda}_c^-$ decay modes using weight factors equal to the product of the total efficiency and the $\bar{\Lambda}_c^-$ partial decay width.

We estimate the systematic uncertainties associated with the fit by changing the order of the background polynomial, the fitting range, and by enlarging the mass resolution by 20%. The observed deviations are taken as systematic uncertainties. Uncertainties on $\mathcal{B}(\bar{\Lambda}_c^- \to \bar{p} K^+ \pi^-)$ and $\Gamma(\bar{\Lambda}_c^- \to \bar{p} K_S^0)/\Gamma(\bar{\Lambda}_c^- \to \bar{p} K^+ \pi^-)$ are taken from Ref. [22]. The final uncertainties on the two $\bar{\Lambda}_c^-$ partial decay widths are summed in quadrature with the reconstruction efficiency as a weighting factor. The uncertainty due to the B tagging efficiency is 4.2% [36]. The uncertainty on $\mathcal{B}[\Upsilon(4S) \to B^+ B^-]$ is 1.2% [22]. The systematic uncertainty on $N_{\Upsilon(4S)}$ is 1.37% [37]. For the Ξ_c^0 branching fractions and the corresponding ratios, some common systematic uncertainties cancel, including tracking, particle identification, $\bar{\Lambda}_c^-$ branching fractions, Λ and K_S^0 selections, and N_{B^-}. The sources of uncertainty summarized in Table I are assumed to be independent and thus are added in quadrature to obtain the total systematic uncertainty.

In summary, based on $(772 \pm 11) \times 10^6$ $B\bar{B}$ pairs collected by Belle, we have performed an analysis of $B^- \to \bar{\Lambda}_c^- \Xi_c^0$ inclusively with respect to the Ξ_c^0 decay using a hadronic B-tagging method based on a full reconstruction algorithm [32], and exclusively for Ξ_c^0 decays into $\Xi_c^- \pi^+$, $\Lambda K^- \pi^+$, and $p K^- K^- \pi^+$ final states. We report the first measurements of the absolute branching fractions

$$\mathcal{B}(\Xi_c^0 \to \Xi^- \pi^+) = (1.80 \pm 0.50 \pm 0.14)\%,$$
$$\mathcal{B}(\Xi_c^0 \to \Lambda K^- \pi^+) = (1.17 \pm 0.37 \pm 0.09)\%,$$
$$\mathcal{B}(\Xi_c^0 \to p K^- K^- \pi^+) = (0.58 \pm 0.23 \pm 0.05)\%.$$

The measured $\mathcal{B}(\Xi_c^0 \to \Xi^- \pi^+)$ is consistent with the theoretical predictions within uncertainties [15–17]. The $\mathcal{B}(B^- \to \bar{\Lambda}_c^- \Xi_c^0)$ is measured for the first time to be

$$\mathcal{B}(B^- \to \bar{\Lambda}_c^- \Xi_c^0) = (9.51 \pm 2.10 \pm 0.88) \times 10^{-4}.$$

For the above branching fractions, the first uncertainties are statistical and the second systematic. The product branching fractions are $\mathcal{B}(B^- \to \bar{\Lambda}_c^- \Xi_c^0)\mathcal{B}(\Xi_c^0 \to \Xi^- \pi^+) = (1.71 \pm 0.28 \pm 0.15) \times 10^{-5}$, $\mathcal{B}(B^- \to \bar{\Lambda}_c^- \Xi_c^0)\mathcal{B}(\Xi_c^0 \to \Lambda K^- \pi^+) = (1.11 \pm 0.26 \pm 0.10) \times 10^{-5}$, and $\mathcal{B}(B^- \to \bar{\Lambda}_c^- \Xi_c^0)\mathcal{B}(\Xi_c^0 \to pK^-K^-\pi^+) = (5.47 \pm 1.78 \pm 0.57) \times 10^{-6}$. The first two are consistent with previous measurements [23,24] with improved precision. Our results supersede previous ones from Belle [23]. The ratios of $\mathcal{B}(\Xi_c^0 \to \Lambda K^- \pi^+)/\mathcal{B}(\Xi_c^0 \to \Xi^- \pi^+)$ and $\mathcal{B}(\Xi_c^0 \to pK^-K^-\pi^+)/\mathcal{B}(\Xi_c^0 \to \Xi^- \pi^+)$ are $0.65 \pm 0.18 \pm 0.04$ and $0.32 \pm 0.12 \pm 0.07$, respectively, which are consistent with world-average values 1.07 ± 0.14 and 0.34 ± 0.04 [22] within uncertainties. For the above branching fractions, the first uncertainties are statistical and the second systematic. Our measured Ξ_c^0 branching fractions, e.g., that for $\Xi_c^0 \to \Xi^- \pi^+$, can be combined with Ξ_c^0 branching fractions measured relative to $\Xi_c^0 \to \Xi^- \pi^+$ to yield other absolute Ξ_c^0 branching fractions.

We thank Professor Fu-sheng Yu for useful discussions and comments. Y. B. L. acknowledges the support from the China Scholarship Council (201706010043). We thank the KEKB group for excellent operation of the accelerator; the KEK cryogenics group for efficient solenoid operations; and the KEK computer group, the NII, and PNNL/EMSL for valuable computing and SINET5 network support. We acknowledge support from MEXT, JSPS and Nagoya's TLPRC (Japan); ARC (Australia); FWF (Austria); the National Natural Science Foundation of China under Contracts No. 11475187, No. 11521505, No. 11575017, No. 11761141009; the CAS Center for Excellence in Particle Physics (CCEPP); MSMT (Czechia); CZF, DFG, EXC153, and VS (Germany); DST (India); INFN (Italy); MOE, MSIP, NRF, RSRI, FLRFAS project and GSDC of KISTI and KREONET/GLORIAD (Korea); MNiSW and NCN (Poland); MSHE, Agreement No. 14.W03.31.0026 (Russia); ARRS (Slovenia); IKERBASQUE (Spain); SNSF (Switzerland); MOE and MOST (Taiwan); and DOE and NSF (U.S.).

---

[1] H. Y. Cheng, Front. Phys. **10**, 101406 (2015).
[2] B. Bhattacharya and J. L. Rosner, Phys. Rev. D **77**, 114020 (2008).
[3] H. Y. Cheng and C. W. Chiang, Phys. Rev. D **81**, 074021 (2010).
[4] H. N. Li, C. D. Lu, and F. S. Yu, Phys. Rev. D **86**, 036012 (2012).
[5] S. Müller, U. Nierste, and S. Schacht, Phys. Rev. D **92**, 014004 (2015).
[6] A. Zupanc *et al.* (Belle Collaboration), Phys. Rev. Lett. **113**, 042002 (2014).
[7] M. Ablikim *et al.* (BESIII Collaboration), Phys. Rev. Lett. **116**, 052001 (2016).
[8] J. G. Körner, G. Krämer, and J. Wilrodt, Z. Phys. C **2**, 117 (1979).
[9] T. Uppal, R. C. Verma, and M. P. Khanna, Phys. Rev. D **49**, 3417 (1994).
[10] G. Kaur and M. P. Khanna, Phys. Rev. D **44**, 182 (1991).
[11] Q. P. Xu and A. N. Kamal, Phys. Rev. D **46**, 270 (1992).
[12] P. Zenczykowski, Phys. Rev. D **50**, 402 (1994).
[13] J. G. Körner and G. Krämer, Z. Phys. C **55**, 659 (1992).
[14] H. Y. Cheng and B. Tseng, Phys. Rev. D **46**, 1042 (1992); **55**, 1697(E) (1997).
[15] H. Y. Cheng and B. Tseng, Phys. Rev. D **48**, 4188 (1993).
[16] D. Wang, P.-F. Guo, W.-H. Long, and F.-S. Yu, J. High Energy Phys. 03 (2018) 066.
[17] H. J. Zhao, Y. K. Hsiao, and Y. Yao, arXiv:1811.07265.
[18] T. Lesiak *et al.* (Belle Collaboration), Phys. Lett. B **605**, 237 (2005); **617**, 198(E) (2005).
[19] R. Aaij *et al.* (LHCb Collaboration), Phys. Rev. Lett. **113**, 242002 (2014).
[20] R. Aaij *et al.* (LHCb Collaboration), Phys. Rev. D **93**, 092007 (2016).
[21] H. Y. Cheng, C. K. Chua, and S. Y. Tsai, Phys. Rev. D **73**, 074015 (2006).
[22] M. Tanabashi *et al.* (Particle Data Group), Phys. Rev. D **98**, 030001 (2018).
[23] R. Chistov *et al.* (Belle Collaboration), Phys. Rev. D **74**, 111105 (2006).
[24] B. Aubert *et al.* (*BABAR* Collaboration), Phys. Rev. D **77**, 031101 (2008).
[25] Inclusion of charge-conjugate states is implicit unless otherwise stated.
[26] A. Abashian *et al.* (Belle Collaboration), Nucl. Instrum. Methods Phys. Res., Sect. A **479**, 117 (2002); also, see detector section in J. Brodzicka *et al.*, Prog. Theor. Exp. Phys. (**2012**) 04D001.
[27] S. Kurokawa and E. Kikutani, Nucl. Instrum. Methods Phys. Res., Sect. A **499**, 1 (2003), and other papers included in this volume; T. Abe *et al.*, Prog. Theor. Exp. Phys. **2013**, 03A001 (2013), and references therein.
[28] D. J. Lange, Nucl. Instrum. Methods Phys. Res., Sect. A **462**, 152 (2001).
[29] T. Sjöstrand, P. Edén, C. Friberg, L. Lönnblad, G. Miu, S. Mrenna, and E. Norrbin, Comput. Phys. Commun. **135**, 238 (2001).
[30] R. Brun *et al.*, GEANT 3: user's guide Geant 3.10, Geant 3.11, CERN Report No. DD/EE/84-1, 1984.
[31] Y. B. Li *et al.* (Belle Collaboration), Eur. Phys. J. C **78**, 928 (2018).
[32] M. Feindt, F. Keller, M. Kreps, T. Kuhr, S. Neubauer, D. Zander, and A. Zupanc, Nucl. Instrum. Methods Phys. Res., Sect. A **654**, 432 (2011).
[33] H. Albrecht *et al.* (ARGUS Collaboration), Phys. Lett. B **229**, 304 (1989).
[34] Y. Kato *et al.* (Belle Collaboration), Phys. Rev. D **94**, 032002 (2016).
[35] N. Dash *et al.* (Belle Collaboration), Phys. Rev. Lett. **119**, 171801 (2017).
[36] A. Sibidanov *et al.* (Belle Collaboration), Phys. Rev. D **88**, 032005 (2013).
[37] E. Guido *et al.* (Belle Collaboration), Phys. Rev. D **96**, 052005 (2017).